

# On the structure of Lithium-Phosphate glasses doped with iron and vanadium ions

C. ANDRONACHE<sup>a</sup>, M. BALASOIU<sup>b,c,d,\*</sup>, O. L. ORELOVICH<sup>b</sup>, A. V. ROGACHEV<sup>b,d</sup>,  
L. MIHALY-COZMUTA<sup>a</sup>, A.-M. BALASOIU-GAINA<sup>b,e,f</sup>, D. RACOLTA<sup>a</sup>

<sup>a</sup>Technical University of Cluj Napoca, North University Center of Baia Mare, Romania

<sup>b</sup>Joint Institute for Nuclear Research, Dubna, Russia

<sup>c</sup>"Horia Hulubei" National Institute for Nuclear Physics and Engineering, Bucharest-Magurele, Romania

<sup>d</sup>Moscow Institute of Physics and Technology, Dolgoprudny, Russia

<sup>e</sup>West University of Timisoara, Timisoara, Romania

<sup>f</sup>CMCF, Moscow State University, Moscow, Russia

Structural investigations on the glasses from the system  $x(\text{Fe}_2\text{O}_3 \cdot \text{V}_2\text{O}_5) \cdot (100-x)[\text{P}_2\text{O}_5 \cdot \text{Li}_2\text{O}]$  with  $0 < x < 50$  mol%, were accomplished. Scanning electron microscopy and small angle neutron scattering methods were used for the present study. The structural 2D-results from SEM are in good agreement with the 3D-results from SANS. It is found that with the increase of the concentration  $x$  the microstructure features of the system are changing from particulate to fractal.

(Received June 14, 2019; accepted December 10, 2019)

**Keywords:** Lithium-Phosphate glasses, SEM, SANS, microstructure

## 1. Introduction

Glasses containing transition metal ions are important materials for the science, technology, and engineering, for their electrical, optical and magnetic properties that make them suitable for large number of applications in many fields [1-6].

The addition of transition metal oxides such as  $\text{V}_2\text{O}_5$  in phosphate glasses was investigated due to their properties such as low glass transition temperatures, high thermal expansion coefficient, and low melting temperature [7-12].

The obtained systems are new and detailed investigations of the resulted compounds are necessary. In the present paper the microstructure of the glasses from the system  $x(\text{Fe}_2\text{O}_3 \cdot \text{V}_2\text{O}_5) \cdot (100-x)[\text{P}_2\text{O}_5 \cdot \text{Li}_2\text{O}]$  with  $0 < x < 50$  mol%, is studied. Earlier, investigations by means of FT-IR [13] and Raman [14] spectroscopy and Electron Paramagnetic Resonance (EPR) [15], were accomplished on similar samples in order to identify the spectral contribution of each unit component, to point out the role of the iron and vanadium ions, respectively to determine the local structure of these glasses.

The FT-IR results showed that  $\text{Fe}_2\text{O}_3$  and  $\text{V}_2\text{O}_5$  contribute to the structure as network modifiers forming non-bridging oxygen ions. When their concentration increases, also the number of non-bridging oxygen ions increase. At a higher content of iron and vanadium ions, the P=O bonds are breaking, the P-O-P bonds are replaced by P-O-Fe or P-O-V bonds and the  $\text{FeO}_4$  units appear together with the  $\text{FeO}_6$  units [13].

The Raman spectra of the similar glass systems like  $x\text{MeO} \cdot (100-x)[\text{P}_2\text{O}_5 \cdot \text{CaO}]$ , ( $\text{MeO} = \text{Fe}_2\text{O}_3, \text{V}_2\text{O}_5$  or  $(\text{Fe}_2\text{O}_3 \cdot \text{V}_2\text{O}_5)$ ) showed that the addition of  $\text{Fe}_2\text{O}_3$  and  $\text{V}_2\text{O}_5$  in the glass matrix causes a depolymerization of the phosphate chains network and the glass network is changing gradually, with the increasing of iron and vanadium content. For example, the Raman spectra of  $x\text{Fe}_2\text{O}_3 \cdot (100-x)[\text{P}_2\text{O}_5 \cdot \text{CaO}]$  do not present any absorption bands characteristic to  $\text{Fe}_2\text{O}_3$  but its evolution is dependent on the iron content. The Raman spectra of  $x\text{V}_2\text{O}_5 \cdot (100-x)[\text{P}_2\text{O}_5 \cdot \text{CaO}]$  present, besides the bands specific for the matrix, some bands assigned to characteristic vibrations of V-O bonds which are evidenced only for high content of  $\text{V}_2\text{O}_5$  [14].

Samples like  $x\text{MeO} \cdot (100-x)[\text{P}_2\text{O}_5 \cdot \text{CaO}]$ , ( $\text{MeO} = \text{Fe}_2\text{O}_3, \text{V}_2\text{O}_5$  or  $(\text{Fe}_2\text{O}_3 \cdot \text{V}_2\text{O}_5)$ ), studied by EPR method, show for low content of  $\text{V}_2\text{O}_5$  that all the spectra present a hyperfine structure typical for isolated  $\text{V}^{4+}$  ions. When the  $\text{V}_2\text{O}_5$  content increase, the EPR absorption signal showing hyperfine structure superposed by a broad line without hyperfine structure characteristic for clustered ions. At high  $\text{V}_2\text{O}_5$  content, the vanadium hyperfine structure disappears and only the broad line can be observed in the spectra [15]. For the glasses  $x(\text{Fe}_2\text{O}_3) \cdot (100-x)[\text{P}_2\text{O}_5 \cdot \text{CaO}]$ , the composition dependence of the absorption line intensity shows an increasing up to  $x = 20$  mol% and for higher concentrations decreases [16]. For the  $x(\text{Fe}_2\text{O}_3) \cdot (100-x)[\text{P}_2\text{O}_5 \cdot \text{Li}_2\text{O}]$  glass systems with  $x > 10$  mol%  $\text{Fe}_2\text{O}_3$  concentration range, isolated  $\text{Fe}^{3+}$  ions subjected to strong crystalline field effects were detected [16].

The present work reports on the structural investigations of  $x(\text{Fe}_2\text{O}_3 \cdot \text{V}_2\text{O}_5) \cdot (100-x)[\text{P}_2\text{O}_5 \cdot \text{Li}_2\text{O}]$  with  $0 < x < 50$  mol% by means of scanning electron microscopy (SEM), and small-angle neutron scattering (SANS). These methods are used in order to obtain complementary information about the influence of local symmetry and interactions between iron and vanadium ions with the increasing of  $\text{Fe}_2\text{O}_3 \cdot \text{V}_2\text{O}_5$  content in the  $\text{P}_2\text{O}_5 \cdot \text{Li}_2\text{O}$  glass matrix on the morphology and microstructure of the system.

## 2. Experimental

### 2.1. Samples preparation

For the samples preparation  $(\text{NH}_4)_2\text{HPO}_4$ ,  $\text{Li}_2\text{CO}_3$ ,  $\text{Fe}_2\text{O}_3$  and  $\text{V}_2\text{O}_5$  of reagent grade purity were used.

Samples were prepared as in the case of other phosphate glasses [17-19] by weighing suitable proportions of components, powder mixing and mixture melting in sintered corundum crucibles at 1250°C for 5 minutes. The mixtures were put into the furnace directly at this temperature. The melts were poured onto stainless steel plates.

Five samples of  $x(\text{Fe}_2\text{O}_3 \cdot \text{V}_2\text{O}_5) \cdot (100-x)[\text{P}_2\text{O}_5 \cdot \text{Li}_2\text{O}]$  with  $x=0; 5; 20; 35; 50$  mol% were obtained.

### 2.2. X-ray diffraction

The samples were analyzed by XRD method using PANalitical X-ray diffractometer Empyreanin Cu-radiation with scanning step  $\sim 0.026$  degree. The X-ray patterns of the investigated samples are characteristic for vitreous systems. No crystalline phase was observed up to 50 mol% ( $\text{Fe}_2\text{O}_3 \cdot \text{V}_2\text{O}_5$ ).

### 2.3. Scanning electron microscopy

Scanning electron microscopy analysis was accomplished at the FESEM (Hitachi SU8020) instrument in function at the Center of Applied Physics of FLNR-JINR.

### 2.4. Small angle neutron scattering

Small angle neutron scattering experiments consist in measuring the intensity of the scattered neutrons versus the amplitude of the scattering wavevector defined by  $Q = (4\pi/\lambda)\sin(\theta/2)$ , where  $\theta$  is the scattering angle and  $\lambda$  is the neutron wavelength.

SANS measurements were performed on the time-of-flight YuMO spectrometer with two detector modes [20-23] in function at the IBR-2 high flux pulsed reactor (JINR Dubna).

The SONIX+ software system accomplished the control of the spectrometer [24]. The experiments were carried out at sample-to-detector distances of 5.28m and 13.04 m, resulting in a  $Q$  range of  $0.006 \div 0.06 \text{ \AA}^{-1}$ . Background scattering on the substrate and on the vanadium reference sample was accounted by using SAS software (small angle neutron scattering intensity in absolute units of  $\text{cm}^{-1}$ ) [25]. Experiment was carried out at a room temperature.

## 3. Results and discussion

### 3.1. SEM-analysis

SEM was used to study the morphological features of  $x(\text{Fe}_2\text{O}_3 \cdot \text{V}_2\text{O}_5) \cdot (100-x)[\text{P}_2\text{O}_5 \cdot \text{Li}_2\text{O}]$  with  $x=0; 5; 20; 35; 50$  mol% samples (Fig. 1).

For  $x=0$  (Fig.1a) and  $x=5$ mol% (Fig.1b) the image of the sample presents mainly round and ellipsoidal drop-like aspect. Beginning with  $x=20$ mol% the surface of the samples reveals the presence of pronounced big irregular structures with sharp edges (Fig. 1 c, d, e). From the SEM images it can be concluded that the increase of  $\text{Fe}_2\text{O}_3 \cdot \text{V}_2\text{O}_5$  concentration induce the growth of these structures.

### 3.2. SANS-analysis

Structural analysis in the volume of the samples was accomplished using SANS method.

It is well known that, identical SANS curves or identical SANS curve regions can be obtained for very different nanosystems. In order to choose one or other of the possible SANS modeling methods, it is essential to know additional structural information such as electron microscopy, SEM or TEM (transmission electron microscopy). In the following, we present a preliminary, possible interpretation of the experimental data of the measured SANS curves, taking into account the information obtained from the scanning electron microscopy images (Fig.1).

In Fig. 2 the SANS experimental curves for  $x$  varying from 0 to 50 mol% are depicted.

In function of the  $x$  value, two structural regimes are revealed in the range of scattering vector  $0.006 < Q < 0.085 \text{ \AA}^{-1}$ :

- (i) for  $x=0$  and 5 mol%, a structural regime characterizing particulate structures;
- (ii) for  $x=20; 35; 50$  mol%, a structural regime characterizing fractal structures, due to the power law behavior of the curves, is detected.

Further the cases of  $x=0$  and 50 mol% will be analyzed.

In Fig. 2 the SANS experimental curves for  $x$  varying from 0 to 50 mol% are depicted.

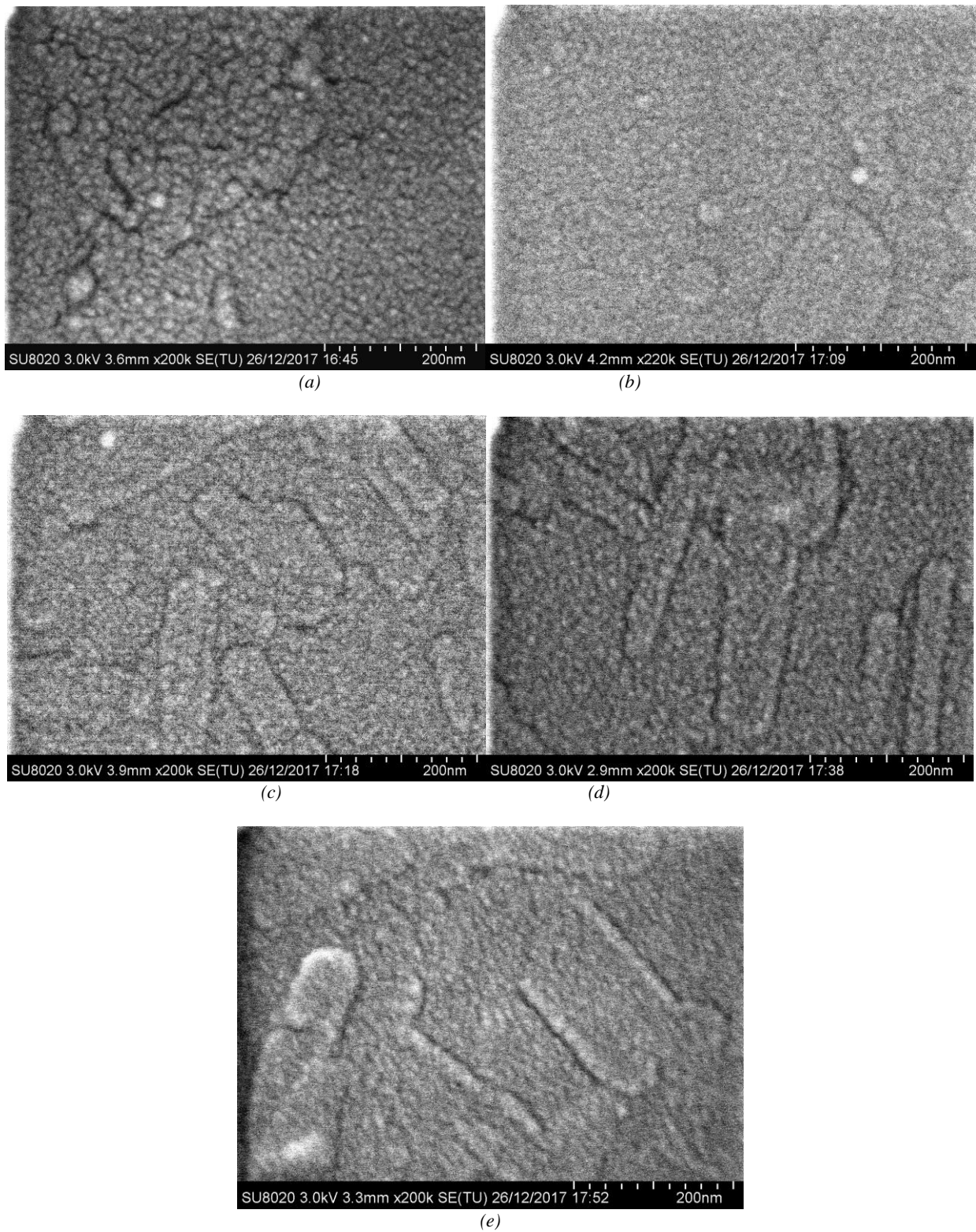


Fig. 1. SEM images of  $x(Fe_2O_3 \cdot V_2O_5) \cdot (100-x)[P_2O_5 \cdot Li_2O]$ , measured on FESEM SU8020 type microscope: (a)  $x=0$ ; (b)  $x=5\%$ ; (c)  $x=20\%$ ; (d)  $x=35\%$ ; (e)  $x=50\%$

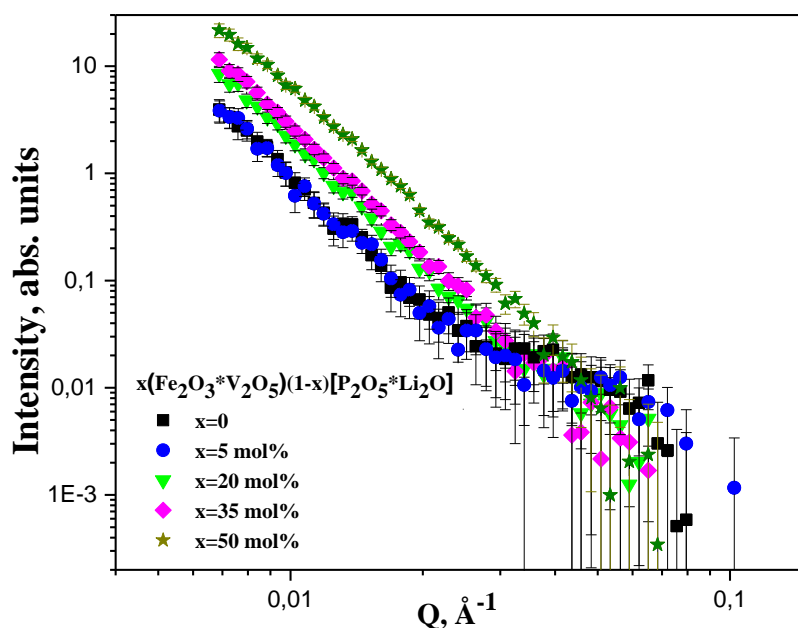


Fig. 2. SANS experimental curves for  $x(\text{Fe}_2\text{O}_3\cdot\text{V}_2\text{O}_5)\cdot(100-x)[\text{P}_2\text{O}_5\cdot\text{Li}_2\text{O}]$  with  $0 < x < 50$  mol% samples obtained at YuMO instrument in function at IBR-2 reactor

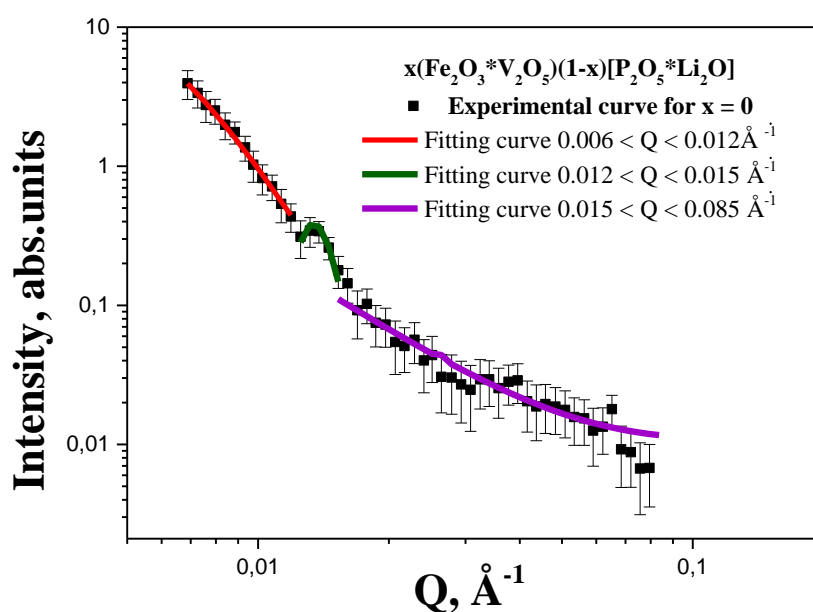


Fig. 3. SANS experimental and fitting curves for  $x(\text{Fe}_2\text{O}_3\cdot\text{V}_2\text{O}_5)\cdot(100-x)[\text{P}_2\text{O}_5\cdot\text{Li}_2\text{O}]$  with  $x = 0$  sample

### 3.2.1. Analysis of SANS experimental curve for $x=0$

The experimental data for  $x=0$  were modeled in the whole  $Q$  region by using form factors for different morphological shapes to obtain the size parameters best describing the scattering signal [26].

In Fig.3 SANS experimental and fitting curves for sample with  $x=0$  are presented.

Using the FITTER program [27] three-form factors were found in the range of  $0.006 < Q < 0.085 \text{ \AA}^{-1}$ , as follows:

$$(a) \quad 0.006 < Q < 0.012 \text{ \AA}^{-1}$$

A cylinder having radius  $R$  and length  $H$ , described with the expression,

$$I(Q) = A \int_0^1 \Lambda_1^2(t) \left( QR \sqrt{1-x^2} \right) S^2(QHx/2) dx + B \quad \text{where,}$$

$\Lambda_1(t) = 2J_1(t)/t$ ,  $S(t) = \sin t/t$ ,  $J_1$  is the cylindrical

Bessel function of order 1 and B is the background, best represents the experimental data.

$$I(Q) = A \int_0^1 \int_0^1 \left[ \Phi \left[ Q \sqrt{\left[ \left( a^2 \cos^2 \frac{\pi}{2} x + b^2 \sin^2 \frac{\pi}{2} x \right) (1-y^2) + c^2 y^2 \right]} \right] \right]^2 dx dy + B \quad (1)$$

(b)  $0.012 < Q < 0.015 \text{ \AA}^{-1}$

The form factor of a spherical shell with  $R_1$  the outer radius and  $R_2$  the inner one, described by the following mathematical expression,

$$I(Q) = A \left[ \Phi(QR_1) - \left( \frac{R_2}{R_1} \right)^3 \Phi(QR_2) \right]^2 + B$$

where  $\Phi(t) = 3 \frac{\sin t - t \cos t}{t^3}$  and B is the background, is determined.

(c)  $0.015 < Q < 0.085 \text{ \AA}^{-1}$

A three axial ellipsoid with half-axes a, b, c, described with the expression (1)

where,  $\Phi(t) = 3 \frac{\sin t - t \cos t}{t^3}$ ; B is the background;

$A = I(0)$ , is obtained.

In Table 1, the structural models and obtained dimensions are summarized.

Table 1. Fitting models and structural dimensions

Q-range [ $\text{\AA}^{-1}$ ]	Model	Dimensions [ $\text{\AA}$ ]
0.006 ÷ 0.012	Cylinder	$R = 6145.8$ $L = 402$
0.012 ÷ 0.015	Spherical shell	$R_1 = 693.8$ $R_2 = 364.8$
0.015 ÷ 0.085	Three axial ellipsoid	$a = 2964.1$ $b = 30.2$ $c = 1241.9$

### 3.2.2. Analysis of SANS experimental curve for $x=50 \text{ mol\%}$

In Fig. 4 the log-log SANS experimental curve for the sample of  $x(\text{Fe}_2\text{O}_3 \cdot \text{V}_2\text{O}_5) \cdot (100-x)[\text{P}_2\text{O}_5 \cdot \text{Li}_2\text{O}]$  with  $x=50 \text{ mol\%}$  is represented.

The curve is composed from two distinct parts, whose behaviors are like  $Q^{-\alpha}$ :

- (i) for  $0.006 \leq Q \leq 0.018 \text{ \AA}^{-1}$ ,  $\alpha = 3.7$
- (ii) for  $0.02 \leq Q \leq 0.05 \text{ \AA}^{-1}$ ,  $\alpha = 4.05$

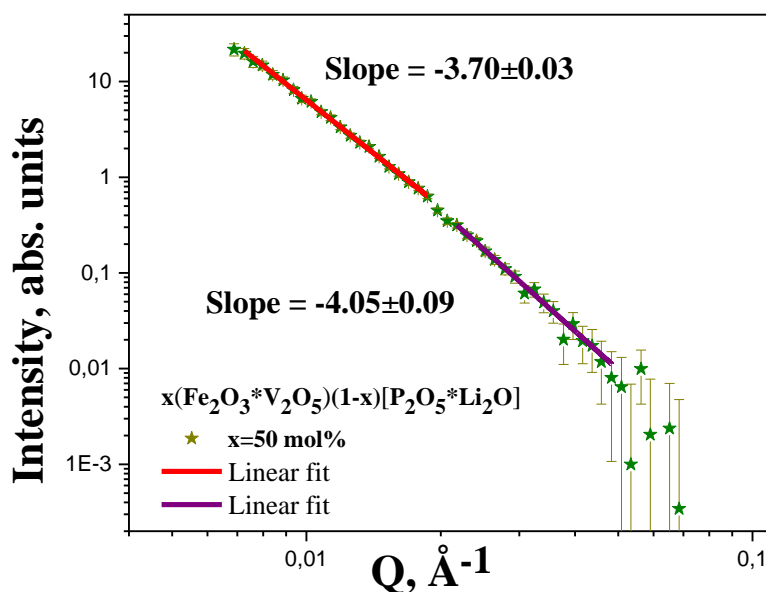


Fig. 4. SANS experimental and fitting curves for  $x(\text{Fe}_2\text{O}_3 \cdot \text{V}_2\text{O}_5) \cdot (1-x)[\text{P}_2\text{O}_5 \cdot \text{Li}_2\text{O}]$  with  $x = 50$  mol% sample

The power-law dependence of the scattering intensity  $I(Q) \approx Q^{-\alpha}$  arising as a linear dependence on a double logarithmic plot in a definite  $Q$  - range is called a fractal region [28, 29]. A succession of power-law decays with different exponents in small-angle scattering experimental data, point out on the presence in the sample of a few fractal structures at different scales [30].

If the power-law exponent is  $\alpha < 3$ , the investigated sample is a mass fractal with the fractal dimension  $D_m = \alpha$ , while if  $3 < \alpha < 4$ , then the sample presents characteristics of a surface fractal with the fractal dimension  $D_s = 6 - \alpha$ . The exponent  $\alpha \cong 4$  is specific for smooth surfaces.

In our case:

(i) for  $\alpha = 3.7$ , the system exhibits the behavior of a surface fractal object with the fractal dimension  $D_s = 2.3$

(ii) for  $\alpha \cong 4$ , the system is formed from scatterer objects with sharp smooth interfaces.

#### 4. Conclusions

Structural investigations on the glasses from the system  $x(\text{Fe}_2\text{O}_3 \cdot \text{V}_2\text{O}_5) \cdot (1-x)[\text{P}_2\text{O}_5 \cdot \text{Li}_2\text{O}]$  with  $0 < x < 50$  mol%, were accomplished. X-ray diffraction, scanning electron microscopy and small angle neutron scattering methods were applied for the study. The X-ray patterns of the investigated samples are characteristic for vitreous systems. No crystalline phase was observed up to 50 mol% ( $\text{Fe}_2\text{O}_3 \cdot \text{V}_2\text{O}_5$ ).

It was obtained, that at the nano length scales, with the increase of the concentration  $x$  the microstructure features of the system are changing from particulate to fractal. The cases of  $x=0$  and 50 mol% are detailed analyzed by SANS. Morphological dimensions of the

initial system are determined. The structural 2D-results from SEM are in good agreement with the spatial organizations results from SANS.

#### Acknowledgements

RO-JINR Projects Nos.323, 322 items 12, 67, 121 and 396, 397 items 4, 67 are acknowledged.

#### References

- [1] A. Hirofumi, O. Satoshi, F. Koji, M. Shunsuke, T. Katsuhisa, Phys. Rev. B **80**, 134408 (2009).
- [2] T. Sankarappa, G. B. Devidas, M. P. Kumar, S. Kumar, B. V. Kumar, J. Alloys Compd. **469**, 576 (2009).
- [3] W. J. Chung, J. Choi, Y. G. Choi, J. Alloys Compd. **505**, 661 (2010).
- [4] K. Srilatha, K. Sambasiva Rao, Y. Gandhi, V. Ravikumar, N. Veeraiah, J. Alloys Compd. **507**, 391 (2010).
- [5] K. A. Aly, Y. B. Saddeek, I. M. El. Kashef, J. Optoelectron. Adv. M. **19**(9-10), 623 (2017).
- [6] Wanzhen Yang, Yang Liu, Huiqian Huang, Jiahui Zhang, Junyan Hou, Tao Zheng, Optoelectron. Adv. Mat. **12**(11-12), 727 (2018).
- [7] J. Y. Ding, P. Y. Shih, S. W. Yung, K. L. Hsu, T. S. Chin, Mat. Chem. Phys. **82**, 61(2003).
- [8] F. Zaera, J. Mater. Chem. **18**, 3521 (2008).
- [9] R. Lakshmikantha, R. Rajaramakrishna, R. V. Anavekar, N. H. Ayachi, Can. J. Phys. **90**, 235 (2012).

- [10] A. I. Nicula, E. Culea, I. Lupsa. *J. Non-Cryst. Solids* **79**, 325 (1986).
- [11] V. Prilepov, P. Gashin, M. Popescu, V. Zalamai, D. Spoiala, P. Ketrush, N. Nasedchina, *J. Optoelectron. Adv. M.* **19**(5-6) 400 (2017).
- [12] M. Ghasemloo, M. T. Hosseinnejad, M. Ettehadi Abari, *J. Optoelectron. Adv. M.* **20**(9-10), 566 (2018).
- [13] I. Ardelean, C. Andronache C. Campean, *Modern Physics Letters B* **20**, 105 (2006).
- [14] C. Andronache, *Modern Physics Letters B* **24**, 2007 (2010).
- [15] C. Andronache, *Materials Chemistry and Physics* **136**, 281 (2012).
- [16] C. Andronache, M. Balasoiu, D. Racolta, *TIM 2018 Physics Conference, Book Series: AIP Conference Proceedings* 2071, (2019).
- [17] C. Andronache, D. Racolta, *AIP Conference Proceedings* **1634**, 115 (2014).
- [18] C. Andronache, M. Balasoiu, D. Racolta, *Russian J. of Phys. Chem. A* **91**, 2686 (2017).
- [19] I. Ardelean, C. Andronache, C. Cimpean, P. Pascuta, *Modern Physics Letters B* **20**, 105 (2006).
- [20] Yu. M. Ostanevich, *Makromol. Chem., Macromol. Symp.* **15**, 91 (1988).
- [21] A. I. Kuklin, A. Kh. Islamov, V. I. Gordeliy, *Neutron News* **16**(3), 16 (2005).
- [22] A. I. Kuklin, D. V. Soloviov, A.V. Rogachev et al., *Journal of Physics: Conference Series* **291**(7), 012013 (2011).
- [23] A. I. Kuklin, A. I. Ivankov, D. V. Soloviov, A. V. Rogachev et al., *Journal of Physics: Conference Series* **994**(7), 012016 (2018).
- [24] A. S. Kirilov, *JINR Communication E10-2017-89*(5), (2017); <https://sonix.jinr.ru/wiki/doku.php?id=en:index>
- [25] A. G. Soloviev, T. M. Solovjeva, O. I. Ivankov, D. V. Soloviov, A.V. Rogachev, A. I. Kuklin, *Journal of Physics: Conf. Series* **848**(7), 012020 (2017).
- [26] L. A. Feigin, D. I. Svergun, *Structure Analysis by Small Angle X-Ray and Neutron Scattering*, Plenum Press, 1987.
- [27] A. G. Soloviev, T. N. Murugova, A. H. Islamov, A. I. Kuklin, *Journal of Physics: Conference Series* **351**(15), 012027 (2012) <https://wwwinfo.jinr.ru/programs/jinrlib/fitter/indexe.html>
- [28] A. Yu. Cherny, E. M. Anitas, A. I. Kuklin, M. Balasoiu, V. A. Osipov, *J. Surf. Investig. X-ray, Synchr. Neutron Techniques* **4**, 903 (2010).
- [29] A. Yu. Cherny, E. M. Anitas, A. I. Kuklin, M. Balasoiu, V. A. Osipov, *J. Appl. Cryst.* **43**, 790 (2010).
- [30] A. Yu. Cherny, E. M. Anitas, V. A. Osipov, A. I. Kuklin, *J. Appl. Cryst.* **47**, 198 (2014).

---

\*Corresponding author: balas@jinr.ru